Available online at www.sciencedirect.com
SCIENCE DIRECT®
Journal of Solid State Chemistry 177 (2004) 1456–1470
JOURNAL OF SOLID STATE CHEMISTRY
http://elsevier.com/locate/jssc

Synthesis, structure, and properties of randomly mixed and layer-ordered $SrMn_{1-x}Ga_xO_{3-\delta}$ perovskites

E.N. Caspi,[a,*] M. Avdeev,[a] S. Short,[a] J.D. Jorgensen,[a] B. Dabrowski,[b] O. Chmaissem,[b] J. Mais,[b] and S. Kolesnik[b]

[a] *Materials Science Division, Argonne National Laboratory, Argonne, IL 60439, USA*
[b] *Department of Physics, Northern Illinois University, DeKalb, IL 60115, USA*

Received 13 January 2003; received in revised form 9 June 2003; accepted 25 November 2003

Abstract

We report the synthesis of $SrMn_{1-x}Ga_xO_{3-\delta}$ perovskite compounds and describe the dependence of their phase stability and structural and physical properties over extended cation and oxygen composition ranges. Using special synthesis techniques, we have extended the solubility limit of Ga^{3+} in the cubic perovskite phase to $x \approx 0.33$. Higher Ga concentrations lead to mixed phases until a single-phase ordered double-perovskite structure is obtained at $x = 0.5$, i.e., $Sr_2MnGaO_{6-\delta}$. In the cubic perovskite phase the maximum oxygen content is $3 - x/2$, which corresponds to 100% Mn^{4+}. All maximally oxygenated solid solution compounds are found to order antiferromagnetically, with the transition temperature linearly decreasing as Ga content increases. Reducing the oxygen content introduces frustration into the magnetic system and a spin-glass state is observed for $SrMn_{0.7}Ga_{0.3}O_{2.5}$ below 30 K. The brownmillerite phase at low oxygen content, Sr_2MnGaO_5, is found to have *Icmm* crystallographic symmetry. At 12 K its magnetic structure is found to order in the *Icm′m′* magnetic symmetry corresponding to a G-type antiferromagnetic structure of Mn^{3+} ions. At higher oxygen content, $Sr_2MnGaO_{5.5}$ is found to have *Cmmm* crystallographic symmetry with disordered oxygen vacancies. At 12 K two competing long-range magnetic structures are found for the Mn^{4+} sublattice having $C_Pm'm'm$ symmetry (G-type), and $C_Pm'm'm$ symmetry (C-type), together with a G-type short-range magnetic correlations.

Keywords: Perovskites; Neutron powder diffraction; Crystal structure; Magnetic structure

1. Introduction

Perovskite manganites have been recently investigated in great detail because of remarkable electronic, magnetic, and structural properties resulting from competing charge, exchange, and phonon interactions [1]. The effects of long-range and local structural order on the properties have been studied extensively for the mixed valent manganites $RE_{1-x}A_xMnO_3$ (RE = La–Sm; A = Ca, Sr, Ba) [2–5]. These materials exhibit the properties of most interest when they form with the perovskite (or closely related) crystal structure. Thus, studies of these materials have been limited by the substitution level of the A cation, beyond which formation of the perovskite phase was not possible because of the decreasing average size of the Mn^{3+x} ion and the unfavorable tolerance factor of the desired composition. For this reason, various schemes have been developed for extending the composition range over which the perovskite phase can be formed. For example, using high-temperature synthesis at reduced oxygen pressure followed by low-temperature oxygen annealing, we have recently been able to extend the solubility limits from $x = 0.6$ to 1 for $La_{1-x}Sr_xMnO_{3-\delta}$ and $Pr_{1-x}Sr_xMnO_{3-\delta}$ [6,7].

This paper describes the properties obtained when $SrMnO_{3-\delta}$ is stabilized in the perovskite phase by the substitution of Ga for Mn. The $SrMnO_{3-\delta}$ compound displays two different crystal structures. When synthesized in oxygen or air, $SrMnO_3$ forms in a hexagonal four-layered structure. This phase transforms to the perovskite phase upon heating in air, as described by Negas and Roth [8]. These authors reported that the

*Corresponding author. Physics Department, Nuclear Research Centre—Negev, P.O. Box 9001, 84190 Beer-Sheva, Israel. Fax: +972-8-656-7878.
E-mail address: eladtally@bezeqint.net (E.N. Caspi).

0022-4596/$ - see front matter © 2003 Elsevier Inc. All rights reserved.
doi:10.1016/j.jssc.2003.11.031

perovskite phase is stable above 1440°C where the oxygen content is reduced below 2.72 atoms per unit formula. This low oxygen content stabilizes the perovskite phase because of the reduced formal valence and resulting in larger ionic size of the Mn cation [9]. Thus, a method that stabilizes the perovskite phase [10,11] is the reduction of hexagonal $SrMnO_{3-\delta}$ in Ar at 1450°C, followed by cooling to low temperatures without allowing the increase of the oxygen content, resulting in an oxygen-vacancy ordered $SrMnO_{2.5}$ compound with all Mn^{3+}. The oxygen-deficient perovskites can then be fully oxygenated ($\delta = 0$) in air at low temperatures (e.g., 200–700°C) where cation diffusion is kinetically hindered, to form a kinetically stable perovskite $SrMnO_3$ [6,12,13]. The stability of pure and Ga-substituted $SrMnO_{3-\delta}$ perovskites at temperatures higher than ~800°C was described by the condition $t(x, T, \delta) \leqslant 1$, where t is the composition, temperature, and oxygen-content-dependent tolerance factor [12,13]. For a given composition x, $t(x, T, \delta)$ is an increasing function of temperature and decreasing function of oxygen-vacancy content; thus, it is possible to tune the synthesis conditions of temperature and oxygen pressure to produce the desired perovskite or hexagonal phases.

The ability to stabilize the perovskite phase by substitution of Ga was demonstrated in the strontium ferrites [14], and its La-doped analog $Sr_{1-x}La_xFe_{1-y}Ga_yO_{3-\delta}$ [15]. We report here the synthesis and properties of the Ga-substituted strontium manganite compounds, $SrMn_{1-x}Ga_xO_{3-\delta}$, over the composition range of $0 \leqslant x \leqslant 0.5$ and $0.5x \leqslant \delta \leqslant 0.5$. These compounds can only be synthesized in the perovskite structure using a two-step synthesis technique involving high-temperature synthesis under reducing conditions followed by low-temperature oxygen annealing. Up to Ga concentrations of $x \approx 0.33$, Ga and Mn mix randomly and a simple cubic phase is formed (space group $Pm\bar{3}m$). The maximum oxygen content is with $\delta = 0.5x$, where all of the Mn is in the 4+ valence state. These simple perovskite phases with $\delta = 0.5x$ are antiferromagnets at low temperatures. The transition temperature decreases linearly with the increase of the diamagnetic Ga^{3+} content. Increasing the oxygen vacancies to form $\delta = 0.5$ compositions (where all Mn is in the 3^+ state) introduces frustration in the magnetic symmetry and a spin-glass state is observed for $SrMn_{0.7}Ga_{0.3}O_{2.5}$.

Upon increasing x beyond ~0.33, mixed phases are formed, until a double-perovskite structure with ordered Ga and Mn is formed at $x = 0.5$. This ordered phase, exhibited by various $A_2MnGaO_{6-\delta}$ compounds (A = Sr, Ca; $\delta \approx 1, 0.5$), has been studied by previous authors [16–20]. For the oxygen-reduced compounds ($\delta \approx 1$), these compounds have the brownmillerite structure which consists of layered cation ordering built up from MnO_6 octahedra and GaO_4 tetrahedra [16–21]. Less work has been done on the maximally oxygenated layered compounds with $\delta \approx 0.5$. Based on X-ray diffraction, $Sr_2MnGaO_{5.47}$ was found to adopt the $P4/mmm$ structure with disordered oxygen vacancies in the $GaO_{5.47}$ layer [17]. Pomjakushin et al. [20] reported the same structure for $Sr_2MnGaO_{5.52(2)}$ based on neutron diffraction but also commented that small additional reflections were observed, that could not be indexed using the $P4/mmm$ structure. The magnetic ground state of $Sr_2MnGaO_{5.52(2)}$ was reported to consist of two coexisting antiferromagnetic phases of the C- and G-type structures, with the latter showing only short-range order characteristics [20]. Our results for the layer-ordered compound $Sr_2MnGaO_{6-\delta}$ ($\delta = 0.5$) differ from the previous reports in two ways. We see a small orthorhombic strain leading to a $Cmmm$ structure for $Sr_2MnGaO_{5.5}$. This observation of lower symmetry may explain the unindexed peaks in the diffraction data reported by Pomjakushin et al. [20]. Also, we observe long-range magnetic ordering for both the C- and G-type coexisting magnetic structures, in contrast to the short-range G-type ordering previously observed. We note that both of these magnetic symmetries are consistent with the $Cmmm$ crystallographic symmetry.

2. Experimental procedures

2.1. Synthesis

The objective of this work was to synthesize and characterize samples of polycrystalline $SrMn_{1-x}Ga_xO_{3-\delta}$ with the perovskite structure over the broadest possible range of Ga concentrations. Thus, synthesis was attempted for compositions $x = 0.1$, 0.2, 0.3, 0.4, and 0.5. Samples were synthesized from stoichiometric mixtures of $SrCO_3$, Ga_2O_3, and MnO_2. Pressed powder samples were initially processed using a solid-state reaction method in which they were fired in air several times at various temperatures up to 1400°C for 20 h followed by either slow cooling or quenching. Powder X-ray diffraction (at room temperature using a Rigaku D/MAX diffractometer) was used to examine the synthesis products. This synthesis procedure did not yield single-phase perovskite samples for any composition.

A two-step synthesis method, as has been successful for extending the composition range of other perovskite compounds, was then explored. In the first step, single-phase oxygen-deficient perovskites were obtained from precursors fired three times at 1300–1335°C for 20 h (the higher temperatures being used for higher values of x) in flowing Ar gas (~20 ppm O_2) with regrinding between firings. For the $x = 0.1$, 0.2, and 0.3 compositions, this yielded single-phase oxygen-deficient perovskite samples with oxygen contents of 2.59(2), 2.55(2), and 2.50(2),

respectively. X-ray diffraction data for these samples were indexed using the simple cubic structure. As an example, Fig. 1(a) shows the X-ray diffraction pattern for the $x = 0.3$ sample. Oxygen contents were determined by measuring samples mass increase after annealing in air at 450°C. Neutron powder diffraction was used to verify the oxygen content for $x = 0.3$ (described later). For $x = 0.4$, a single phase was not obtained at any synthesis temperature in flowing Ar. Instead, these samples were a mixture of a perovskite phase with $x \approx 0.3$ and a layer-ordered phase with $x \approx 0.5$. For $x = 0.5$, repeated grindings and firings (4×20 h) at temperatures of 1300–1330°C in Ar yielded a single-phase oxygen-deficient layer-ordered phase, $SrMn_{0.5}Ga_{0.5}O_{2.50(1)}$. Firing at higher temperatures resulted in partial melting of the $x = 0.5$ sample with associated changes of the Mn/Ga stoichiometry.

In a second synthesis step, oxygen was added to these samples by annealing in air or oxygen at temperatures low enough that cation diffusion could not occur. The $x = 0.1-0.4$ samples were annealed in air at 450°C followed by slow cooling. This resulted in final oxygen contents of approximately $3.00 - x/2 \pm 0.01$ ($\delta = x/2$) atoms per formula unit for $x = 0.1-0.3$ samples as determined by neutron powder diffraction (discussed later). These oxygen contents are the maximally oxygenated compositions with formal valences of Ga and Mn of 3+ and 4+, respectively. Fig. 1(b) shows X-ray diffraction pattern of the $x = 0.3$ sample annealed in air. The $SrMn_{0.5}Ga_{0.5}O_{2.50(1)}$ sample was annealed in oxygen at 380°C followed by slowly cooling to room temperature to achieve the fully oxygenated composition $SrMn_{0.5}Ga_{0.5}O_{2.744(4)}$ (this sample is denoted by "ox380"). A second fully oxygenated sample of the same composition (denoted "ox800") was made by doing the final annealing in oxygen on thermogravimetric analysis (TGA) apparatus at 800°C followed by slowly cooling to room temperature. The structure and properties of the layer-ordered compounds ($x = 0.5$) have been discussed by previous authors [16–20]. We obtained some additional information regarding these compounds that will be presented later.

Table 1 summarizes the samples that were used for neutron powder diffraction and magnetic susceptibility measurements. The oxygen contents of these samples were found by refining the oxygen occupancy using the neutron diffraction data for all maximally oxygenated samples and the reduced $x = 0.3$ sample. Using these values as the references, oxygen contents for the other samples were determined from TGA measurements. Many additional samples, made using these same techniques, were used in X-ray diffraction and TGA

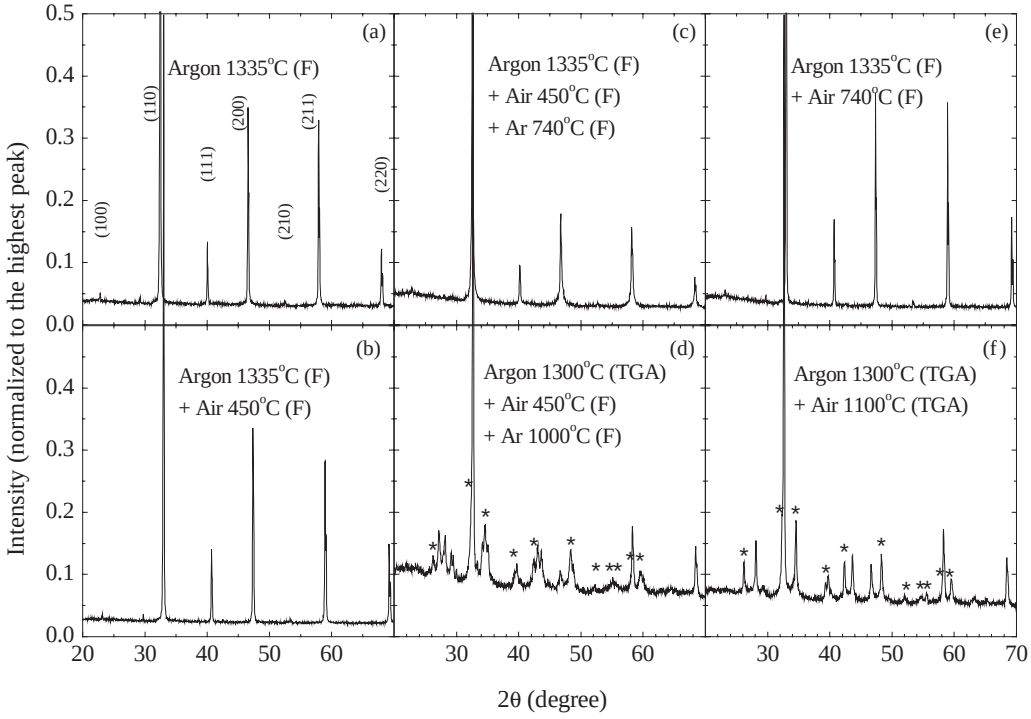

Fig. 1. X-ray diffraction patterns of the $SrMn_{0.7}Ga_{0.3}O_{3-\delta}$ samples that were obtained using the furnaces (F) or TGA apparatus: (a) fired in Ar at 1335°C for 60 h—single phase; (b) fired in Ar at 1335°C and annealed in air at 450°C—single phase; (c) fired in Ar at 1335°C, annealed in air at 450°C and fired in Ar at 740°C for 8 h—single phase; (d) fired in Ar at 1300°C (TGA), annealed in air at 450°C and fired in Ar at 1000°C for 20 h—partially decomposed; (e) fired in Ar at 1335°C and annealed in air at 740°C—single phase; and (f) fired in Ar at 1300°C and annealed in air at 1100°C—partially decomposed. Diffraction peaks corresponding to hexagonal 4-layered impurity phase are marked with asterisks. The small not indexed reflections at 29.7° and 47.5° in 1(a) and 1(b) are diffraction peaks corresponding to the Cu$K\beta$ radiation of the highest intensity Bragg peaks.

Table 1
Samples that were used for neutron powder diffraction and magnetic susceptibility measurements

Sample	Neutron powder diffraction		Magnetic susceptibility
	295 K	12 K	
$SrMn_{0.9}Ga_{0.1}O_{2.93(2)}$	✓	✓	✓
$SrMn_{0.9}Ga_{0.1}O_{2.59(2)}$	—	—	✓
$SrMn_{0.8}Ga_{0.2}O_{2.87(2)}$	✓	✓	✓
$SrMn_{0.8}Ga_{0.2}O_{2.55(2)}$	—	—	✓
$SrMn_{0.7}Ga_{0.3}O_{2.83(2)}$	✓	—	✓
$SrMn_{0.7}Ga_{0.3}O_{2.50(2)}$	✓	✓	✓
$SrMn_{0.5}Ga_{0.5}O_{2.50(2)}$	✓	✓	✓
$SrMn_{0.5}Ga_{0.5}O_{2.744(4)}$ "ox380"	✓	✓	✓
$SrMn_{0.5}Ga_{0.5}O_{2.762(6)}$ "ox800"	✓	—	✓

For samples measured using neutron diffraction, the refined oxygen content is reported. Otherwise, oxygen content was determined by measuring sample mass changes after annealing (see text).

analysis measurements as part of a detailed investigation of the synthesis chemistry (to be described later). The oxygen contents obtained from the neutron data are in agreement with the estimated values obtained from TGA measurements assuming all Mn^{4+} (Mn^{3+}) for fully oxygenated (reduced) samples.

2.2. Thermogravimetric (TGA) measurements

TGA measurements were used to study the behavior of these materials as a function of temperature and oxygen partial pressure in order to understand the synthesis in more detail. Absolute oxygen contents were determined by Rietveld refinement of the oxygen site occupancy using neutron powder diffraction data from reduced or maximally oxygenated samples (to be described later). Hydrogen reduction on the TGA balance cannot be used to determine the absolute oxygen contents because the gallium oxide Ga_2O_3 end product partially decomposes in hydrogen and some Ga evaporates. The oxygen contents determined by neutron powder diffraction were, thus, used as the reference points for TGA measurements of oxygen content vs. temperature in various atmospheres. The oxygen contents determined in this way were self-consistent and were also consistent with results from hydrogen reduction on the Ga-free parent compound, $SrMnO_{3-\delta}$ [12,13]. All TGA measurements were performed on a Cahn TG171 thermobalance. For increased accuracy, samples as large as 1 g (consisting of small chunks) were heated in alumina crucibles suspended on Pt wires. The weights of the samples were measured to a precision of 2 μg. Empty-crucible TGA runs were used for calibration and buoyancy corrections. Reproducibility of the data was checked several times using identical TGA conditions for samples with the same x values.

X-ray powder diffraction (at room temperature using a Rigaku D/MAX diffractometer) was used to determine the structure types present at various conditions of temperature and oxygen partial pressure investigated by TGA. For TGA experiments done in Ar gas, the X-ray samples were obtained by rapidly cooling on the TGA balance. For TGA experiments done in 20% O_2 in Ar or in pure O_2, the sample cannot be cooled rapidly enough on the TGA balance to prevent oxygen uptake. Thus, X-ray samples were produced by duplicating the TGA conditions and sample history in an external furnace and then quenching to room temperature. A large number of samples were investigated by X-ray diffraction; only the results needed to support the key conclusions are presented here.

2.3. Neutron diffraction measurements

Time of flight neutron powder diffraction data were collected on the Special Environment Powder Diffractometer [22] at Argonne's Intense Pulsed Neutron Source. Diffraction data were collected for the maximally oxygenated samples $SrMn_{1-x}Ga_xO_{3-\delta}$ with $x = 0.1$, 0.2, 0.3, and 0.4 at RT ($\sim$295 K), and with $x = 0.1$ and 0.2 at low temperature (LT $\approx$ 12 K; see Table 1). RT and LT diffraction data were also collected for the maximally reduced sample $SrMn_{0.7}Ga_{0.3}O_{2.50(2)}$. In addition, RT diffraction data were collected for the two $Sr_2MnGaO_{\sim 5.5}$ oxygenated samples ("ox380" and "ox800") and the oxygen-deficient Sr_2MnGaO_5 sample. LT diffraction data were collected for Sr_2MnGaO_5 and "ox380" $Sr_2MnGaO_{5.49(1)}$. High-resolution backscattering data ($2\theta = 144.85°$, Bank 1), and intermediate-resolution low-angle scattering data ($2\theta = 44°$, Bank 3), were analyzed using the Rietveld method with the GSAS (EXPGUI) suite [23,24]. Bank 3 data were used for refinements of the LT structures because they contained additional magnetic reflections of significant intensities. Magnetic form-factor coefficients for Mn^{3+} and Mn^{4+} were taken from the International Tables.

2.4. Susceptibility and magnetization measurements

AC susceptibility and static (DC) magnetization were measured using a Physical Property Measurement System 6000 (Quantum Design). Zero-field-cooled (ZFC) magnetizations were measured after cooling in zero magnetic field and switching on a magnetic field of 1 kOe at a low temperature. Field-cooled (FC) magnetizations were measured on cooling in the magnetic field. Remnant magnetizations were measured after cooling in the magnetic field and switching the magnetic field to zero.

3. Results and discussion

3.1. TGA and X-ray diffraction investigation of the synthesis process

The TGA measurements, combined with X-ray diffraction studies of samples quenched from several temperatures and atmospheres, show why a two-step synthesis process is needed to make single-phase samples. Fig. 2 shows the oxygen contents upon heating (1.2°/min) single-phase maximally oxygenated samples in Ar. The maximally oxygenated perovskite compositions, $SrMn_{0.9}Ga_{0.1}O_{2.93(2)}$ and $SrMn_{0.7}Ga_{0.3}O_{2.83(2)}$, begin to lose oxygen near 400°C and, then, in the temperature range 830–1130°C, display plateaus in the oxygen contents of 2.82 and 2.67, respectively. X-ray diffraction studies of $x = 0.1$ and 0.3 samples quenched from various temperatures show that the perovskite phase is maintained before these plateaus are reached (cf. Fig. 1(c)), at which point the materials partially decompose into mixtures of phases that include a hexagonal 4-layered structure as a major impurity phase (Fig. 1(d)) [12,13]. Thus, the perovskite phase is not stable at temperatures above 800–900°C (depending on the Ga content) under reducing conditions of ~20 ppm O_2. Further heating introduces more oxygen vacancies and above 1250°C a reverse transformation to the oxygen-deficient perovskite phase occurs, as confirmed by X-ray diffraction data. Single-phase perovskites with large amounts of vacancies, $O_{2.58}$ ($\delta = 0.42$) and $O_{2.50}$ ($\delta = 0.50$) for $x = 0.1$ and 0.3, respectively, are achieved after 14 h holding at 1300°C. Upon quenching to room temperature or cooling to room temperature in a reducing atmosphere so that no oxygen uptake is allowed, a simple cubic perovskite phase with randomly disordered oxygen vacancies is obtained. This structure was confirmed by neutron diffraction measurements for the $x = 0.3$ sample (discussed below). We note that this behavior is similar to that of the $SrMnO_{3-\delta}$ compound, which also requires a two-step synthesis method to achieve the perovskite structure [12,13].

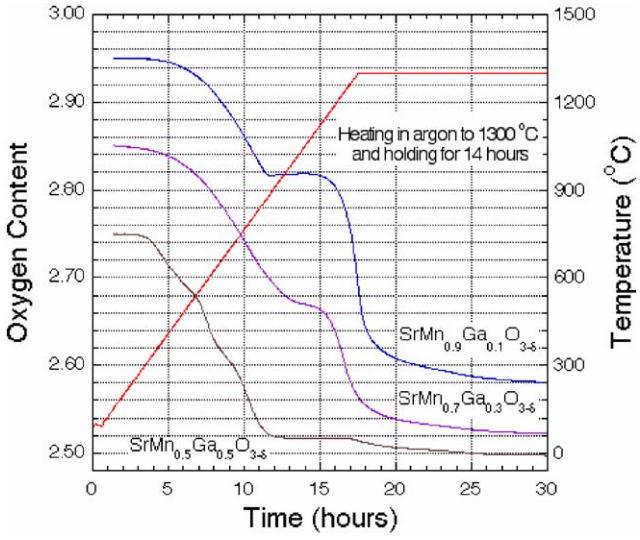

Fig. 2. TGA data showing the oxygen content during heating (1.2°/min) and holding at 1300°C in Ar for the single-phase perovskite samples $SrMn_{1-x}Ga_xO_{3-\delta}$ synthesized using a two-step method (see text).

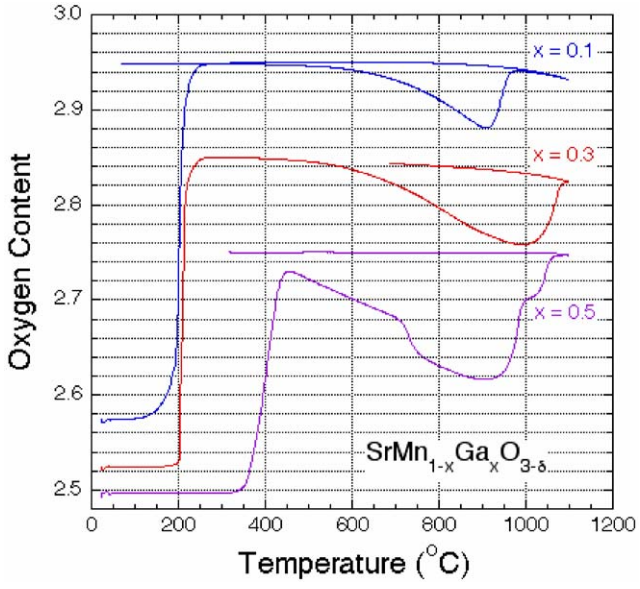

Fig. 3. TGA showing oxygen content during heating (1.0°/min) to 1100°C, holding for 4 h, and cooling (1.0°/min) to RT in 20% O_2/Ar for the single-phase, oxygen-deficient perovskite samples of $SrMn_{1-x}Ga_xO_{3-\delta}$.

The decomposition of the perovskite phase around 800–900°C (depending on Ga content), followed by formation of a single phase at higher temperatures can be understood in terms of diffusion kinetics and tolerance factor arguments. The maximally oxygenated perovskite compounds, $SrMn_{0.9}Ga_{0.1}O_{2.93(2)}$ and $SrMn_{0.7}Ga_{0.3}O_{2.83(2)}$, are metastable at room temperature. When the temperature is raised high enough to enable cation diffusion, decomposition occurs because the tolerance factor required for stability of the

perovskite phase ($t<1$) is not satisfied. Upon further heating, additional oxygen vacancies are formed, thus, decreasing the formal valence of Mn ($(4-3x-2\delta)/(1-x)=3.18$ and 3 for $x=0.1$ and 0.3, respectively) and increasing the ionic size of Mn, R(Mn). As a result, the tolerance factor $t\sim 1/R$(Mn) decreases and requirements for existence of the perovskite phase are satisfied. In a previous paper, these concepts, which can be expressed as a dependence of the tolerance factor on temperature and oxygen content, have been discussed in detail for the parent compound $SrMnO_{3-\delta}$ [12,13].

TGA studies of the oxygen-reduced perovskite samples in oxygen show how the second step of the two-step synthesis process works. Fig. 3 shows the oxygen contents for $SrMn_{0.9}Ga_{0.1}O_{2.58}$ and $SrMn_{0.7}Ga_{0.3}O_{2.50(2)}$ upon heating (1.0°/min) in 20% O_2 in Ar. Oxygen uptake begins abruptly near 200°C and, in the temperature range 250–450°C, the maximal oxygen contents, $3-x/2$ ($\delta=x/2$) atoms per formula unit, corresponding to Mn^{4+}, are achieved. The accuracy with which the oxygen contents deduced from TGA agree with the prediction based on Mn^{4+} validates the calibration of the TGA measurements. On further heating, additional oxygen vacancies form. The oxygen-deficient perovskite phases are kinetically stable in 20% O_2/Ar up to 900–1000°C (cf. Fig. 1(e)). Above this temperature, when cation diffusion is enabled, the single-phase perovskite phase partially decomposes to a multiphase material, as revealed by X-ray diffraction measurements on samples obtained after 4 h hold at 1100°C in TGA, followed by slow cooling (1.0°/min) to room temperature (Fig. 1(f)). The measured changes of oxygen contents and the structural stability of the perovskite phase are essentially the same as for a pure $SrMnO_{3-\delta}$ sample and the behavior can, as for the TGA measurements in Ar, be readily explained in terms of diffusion kinetics and tolerance factor arguments [13].

TGA measurements for the layer-ordered composition, $x=0.5$, also show why a two-step synthesis is needed to make this material in its maximally oxygenated form. Upon heating (1.2°/min) $SrMn_{0.5}Ga_{0.5}O_{2.744(4)}$ in Ar, the sample begins to lose oxygen near 300°C and, then, in the temperature range 500–750°C, displays two weakly defined plateaus of oxygen content near 2.68 and 2.62. X-ray and neutron diffraction shows that these weak plateaus do not correspond to decomposition (as was the case for the $x=0.1$ and 0.3 compositions in the temperature range 900–1250°C). The layer-ordered structure type is maintained. On further heating, a well-defined oxygen-content plateau of 2.52 is observed over the temperature range 900–1200°C. Finally, at 1300°C the fully reduced phase of oxygen content of 2.5 forms. X-ray diffraction measurements (not shown) did not reveal any difference between samples obtained after fast cooling from 900°C and 1300°C. Except for the possibility of oxygen-vacancy ordering not seen by X-ray diffraction, these TGA results show that the layer-ordered $SrMn_{0.5}Ga_{0.5}O_{3-\delta}$ compound is stable in Ar over the entire temperature range up to 1300°C.

TGA measurements in 20% O_2/Ar for $SrMn_{0.5}Ga_{0.5}O_{2.50}$, however, show that this composition is not stable in an oxidizing atmosphere (Fig. 3). Upon heating (1.0°/min) a fully reduced sample, oxygen uptake begins around 350°C, but, at this heating rate, full oxygenation is not achieved before the sample starts to lose oxygen around 450°C. After the oxygen content has decreased to 2.68 at 700°C, more rapid oxygen loss is observed upon further heating followed by a minimum of the oxygen content near 2.62 at 900°C. X-ray diffraction measurements on samples quenched from temperatures below 900°C showed that the layer-ordered structure is maintained. Further heating above ~900°C in 20% O_2/Ar causes the decomposition of the layered Ga/Mn structure by a process that appears to occur in two well-defined steps. This decomposition of a layer-ordered $SrMn_{0.5}Ga_{0.5}O_{3-\delta}$ sample in 20% O_2/Ar is consistent with the inability to synthesize this material in air at any temperature.

In the TGA experiments just described, weak plateaus are observed at oxygen contents near 2.62 and 2.68 for heating in both Ar and 20% O_2 in Ar. In additional experiments (not shown), these weak plateaus were also observed during heating (to 800°C) and cooling in pure oxygen as well as during heating in 1% O_2 to 1200°C. This behavior is reminiscent of that observed for $SrFeO_{3-\delta}$ [25] where the weak plateaus corresponded to ordering of the oxygen vacancies. In that study, neutron powder diffraction was used to understand the vacancy ordering. Such experiments are currently underway for the $SrMn_{0.5}Ga_{0.5}O_{2.5+\delta}$ compound, and will be reported in a future publication.

3.2. Structural and magnetic properties of the solid solution $SrMn_{1-x}Ga_xO_{3-\delta}$ ($0\leqslant x\leqslant 0.3$)

The RT neutron powder diffraction data for maximally oxygenated samples with $x=0.1$, 0.2, and 0.3 confirm that the samples are single phase. Reflections in all patterns were indexed in the cubic perovskite structure, space group $Pm\bar{3}m$, and the structures were refined accordingly using the Rietveld method (cf. Fig. 4). Refined structural parameters are summarized in Table 2. Refined cell parameters as a function of Ga concentration, x, are depicted in Fig. 5, along with the published cell parameter of cubic $SrMnO_3$ [16]. The linear dependence of the cubic cell parameter on x supports the existence of a solid solution of Ga in the $SrMnO_3$ perovskite structure over this composition range.

As mentioned earlier, the RT neutron diffractogram for the maximally oxygenated sample with $x = 0.4$ indicated the presence of more than one phase, leading to the conclusion that this Ga content is above the solubility limit (using our synthesis technique). Extrapolation of the cell parameters in the solid solution range ($0 \leqslant x \leqslant 0.3$) to the value obtained from two-phase Rietveld refinement for the cubic perovskite phase in the multiphase $x = 0.4$ sample (Fig. 5) provides an estimate of the solubility limit of Ga of ~ 0.33. This estimated solubility limit of Ga^{3+} in $SrMnO_{3-\delta}$ ($x \approx 0.33$) is very close to that reported for the solubility of Ga in the strontium ferrites ($x \approx 1/3$) [14] and its La-doped analog $Sr_{1-y}La_yFe_{1-x}Ga_xO_{3-\delta}$ ($x \approx 0.31$ for $y = 0.3$) [15]. Taking into consideration the large ionic size difference between octahedrally coordinated Mn^{4+} and Fe^{4+} (0.67 and 0.725 Å, respectively [9]) this limiting x value could mean that the stability of the perovskite structure in these materials is controlled mainly by the oxygen content.

The LT neutron powder diffraction data for maximally oxygenated samples with $x = 0.1$ and 0.2 show additional reflections to those observed in RT. These new reflections can be described using a G-type

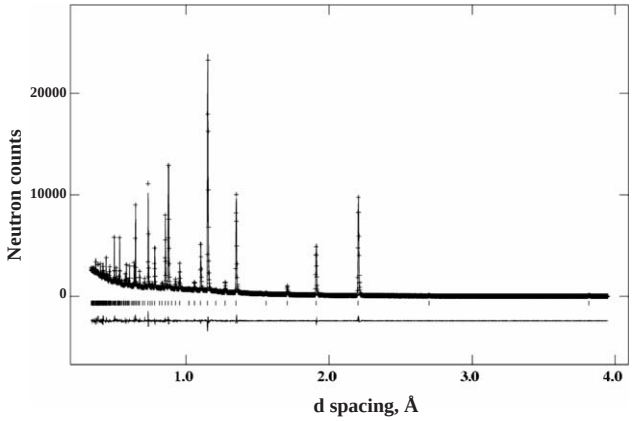

Fig. 4. Best-fit Rietveld refinement using time-of-flight neutron powder diffraction data at RT for nominal $SrMn_{0.9}Ga_{0.1}O_{2.93(2)}$. Plus symbols are observed data from Bank1 ($2\theta = 144.85°$), and continuous lines are the calculated profile and the difference. For structural details see Table 2.

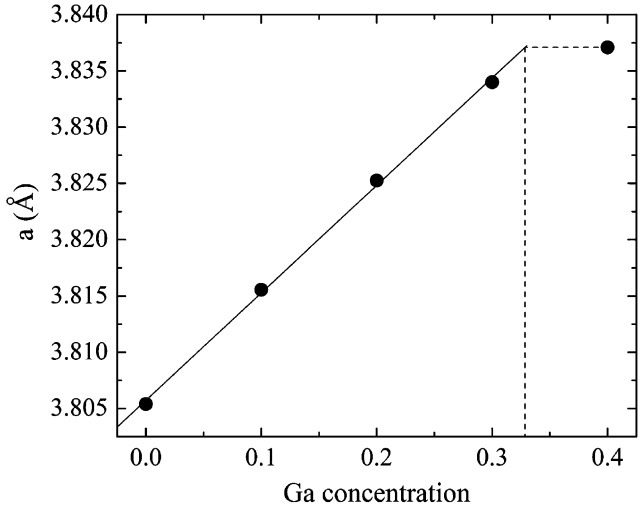

Fig. 5. Lattice parameter a (Å) as a function of Ga concentration, x, in $SrMn_{1-x}Ga_xO_{3-\delta}$ obtained by Rietveld refinement using RT (~ 295 K) neutron diffraction data (Table 2). The solid line is a best fit of the data for Ga concentration in the range 0–0.3. The dashed lines are guides for the eye for determination of solubility limit. Error bars are smaller than the symbol size.

Table 2
RT structural parameters of maximally oxygenated $SrMn_{1-x}Ga_xO_{3-\delta}$ samples as a function of nominal Ga content (x), and the oxygen-deficient $x = 0.3$ ($\delta = 0.5$) sample

x		0.1	0.2	0.3	0.3; $\delta = 0.5$
a (Å)		3.81556(1)	3.82526(1)	3.83400(1)	3.89045(2)
V (Å^3)		55.549(1)	55.973(1)	56.358(1)	58.884(1)
Sr	B (Å^2)	0.62(1)	0.71(2)	0.79(2)	1.42(4)
(Mn,Ga)	Ga SOF	0.09(2)	0.181(3)	0.265(2)	0.24(1)
	B (Å^2)	0.28(2)	0.09(3)	−0.36(4)	−0.26(6)
O	SOF	0.976(5)	0.956(6)	0.943(7)	0.833(7)
	U_{11} (Å^2)	0.54(3)	0.61(4)	0.79(5)	2.6(1)
	$U_{22}(=U_{33})$ (Å^2)	1.14(2)	1.30(3)	1.52(3)	3.8(1)
(Mn,Ga)–O (Å)		1.90778(1)	1.91263(1)	1.91700(1)	1.94523(1)
T_N (K)		190(5)	139(10)	105(2)	—
R_{wp} (%)		6.49	6.15	6.19	4.87
R_{exp} (%)		4.61	4.44	4.39	4.19

Rietveld analyses of neutron diffraction data were performed using the cubic space group $Pm\bar{3}m$, with the following atom positions: Sr at $1b(1/2, 1/2, 1/2)$, (Mn,Ga) at $1a(0,0,0)$, and O at $3d(1/2,0,0)$. SOF is site occupation factor. B (U_{ij}) is the isotropic (anisotropic) thermal displacement parameter. Numbers in parentheses are the standard deviations of the last significant digit. The fitted weighted profile (R_{wp}), and expected (R_{exp}) agreement factors are also given. T_N is the antiferromagnetic transition temperature measured by AC susceptibility.

antiferromagnetic ordering of the Mn ions, similar to the magnetic structure observed in $SrMnO_3$ [6]. The refined Mn^{4+} magnetic moments are 2.32(2) and 2.20(3) μ_B, for $x = 0.1$ and 0.2, respectively.

The AC susceptibilities, χ, vs. temperature are presented in Fig. 6(a) for maximally oxygenated samples with all Mn^{4+}. In the temperature range 50–400 K, the samples show small, nearly temperature-independent susceptibility ($\sim 10^{-5}$ emu/g), with a weak change of slope in the temperature range 100–250 K, depending on the Ga concentration. For $SrMnO_3$ ($x = 0$), this change of slope has been shown to correlate with antiferromagnetic ordering [6]. By analogy, an antiferromagnetic transition is assumed to correspond to the changes of slopes in the susceptibility curves for the Ga-substituted compounds (Fig. 6(a)). For $x = 0.1$ and 0.2 this assumption is in agreement with the neutron diffraction results at LT, described above. The antiferromagnetic transition temperatures (Table 2) were determined from the peak in the derivative $d\chi/dT$ for $x = 0-0.3$. The ordering temperature vs. Ga content, x, is shown in Fig. 7. The increase of susceptibility at lower temperatures is most likely caused by small amounts of magnetic impurities [6].

The RT neutron powder diffraction data for the oxygen-deficient sample $SrMn_{0.7}Ga_{0.3}O_{2.50(2)}$ can be indexed in the cubic perovskite structure, space group $Pm\bar{3}m$ and the structure was refined accordingly using the Rietveld method. Refined structural parameters are summarized in Table 2. The Mn–O distance is significantly larger than the distance refined for the maximally oxygenated sample, in agreement with the reduced oxidation state of Mn^{3+} in the oxygen-deficient sample. In addition, this structure exhibits a random distribution of oxygen vacancies unlike the vacancy-ordered structure found in the oxygen-deficient $SrMnO_{2.5}$ compound [10,11]. This is another evidence for the ability of Ga^{3+} to stabilize the oxygen-vacancy disorder perovskite structure.

The AC susceptibilities of the oxygen-deficient samples (see Table 1) with $x = 0-0.3$ and 0.5 achieved after the synthesis in Ar are shown in Fig. 6(b). The weak transition at $T \approx 370$ K observed for the oxygen-vacancy ordered $SrMnO_{2.5}$ sample ($x = 0$) was previously attributed to a rather complex antiferromagnetic structure [10]. As was mentioned before, X-ray diffraction data for the $x = 0.1$ and 0.2 samples show a cubic structure with disordered oxygen vacancies. The magnetic transitions at $T \approx 230$ K ($x = 0.1$) and $T \approx 140$ K ($x = 0.2$) could not be associated with the same magnetic structure as the $x = 0$ sample since that magnetic structure is associated with the oxygen-vacancy ordered structure. Further neutron diffraction study is needed for the determination of the $x = 0.1$ and 0.2 magnetic structures. The frequency-dependent magnetic susceptibility of the oxygen-deficient

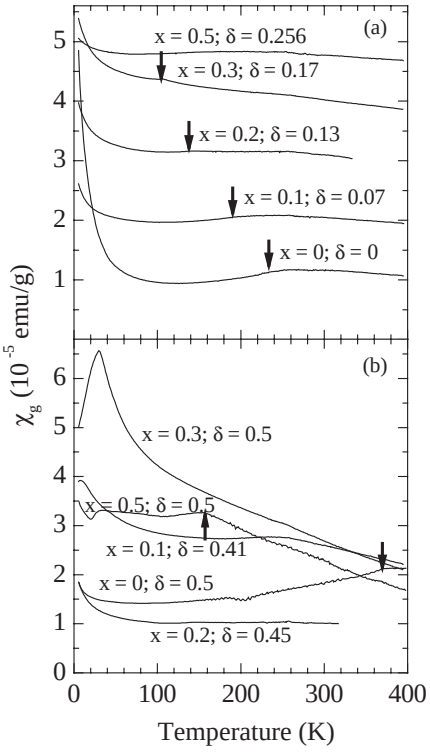

Fig. 6. Temperature dependence of the magnetic susceptibility for $SrMn_{1-x}Ga_xO_{3-\delta}$ with (a) $\delta \approx x/2$ and (b) $\delta \approx 0.5$. For clarity, curves in (a) are shifted by 10^{-5} emu/g with respect to the preceding ones. Antiferromagnetic transition temperatures are marked with arrows.

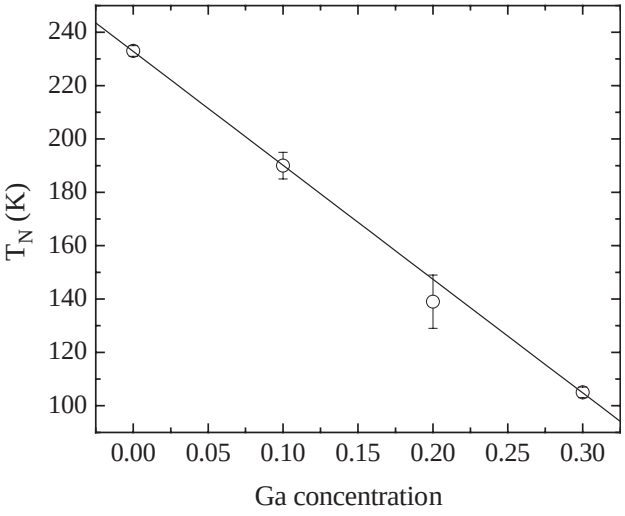

Fig. 7. Antifferomagnetic transition temperature, T_N, as a function of Ga concentration, x, in $SrMn_{1-x}Ga_xO_{3-\delta}$ ($\delta \approx x/2$), deduced from AC magnetic susceptibility measurements (Fig. 6; Table 2). The solid line is a linear best fit to the data.

$SrMn^{3+}_{0.7}Ga^{3+}_{0.3}O_{2.50(2)}$ sample vs. temperature is shown in Fig. 8. The AC-susceptibility measurements show a cusp at a temperature close to 29 K. The position of this cusp depends on the frequency of the AC magnetic field, which is characteristic of spin-glass behavior. We identify the temperature of this cusp as the spin freezing temperature T_f. With increasing frequency, ω, the AC

susceptibility below T_f decreases and T_f shifts towards higher temperatures. A clear divergence between ZFC and FC magnetization is seen below T_f (see inset to Fig. 7). These observations confirm that the observed cusp in the AC susceptibility is related to a spin-glass behavior [26]. A linear fit to T_f vs. $\log\omega$ results in $\Delta T_f/T_f\,\Delta(\log\omega) = 0.009(1)$. The value of this parameter is comparable to other canonical spin-glass systems [26]. Finally, the LT neutron powder diffraction data for the oxygen-deficient sample $SrMn_{0.7}Ga_{0.3}O_{2.50(2)}$ did not show any change in comparison to the RT data, in agreement with the spin-glass state discussed above.

The observed behavior of the magnetic properties in the maximally oxygenated perovskite compounds ($x = 0.1$, 0.2 and 0.3) can be understood in terms of the effects of dilution resulting from the Ga substitution and the associated changes in the oxygen sublattice required because of the limited Mn^{+4} valence. Starting with $SrMnO_3$, replacing Mn with Ga results in weaker magnetic interactions caused by both the dilution of the magnetic ion matrix with randomly distributed diamagnetic Ga^{3+} ions, and the gradual introduction of oxygen vacancies. For the maximally oxygenated solid solution with $0 < x \leqslant 0.3$, the oxygen vacancies are shown in this work to be randomly distributed in the cubic perovskite structure, causing further weakening of the magnetic interactions. Accordingly, the antiferromagnetic transition temperatures for the $SrMn_{1-x}Ga_xO_{\sim 3-0.5x}$ ($0 \leqslant x \leqslant 0.3$) solid solution decrease linearly as x increases (Fig. 7). As was mentioned above, a spin-glass state is clearly indicated by the frequency-dependent AC-susceptibility data for the $SrMn_{0.7}Ga_{0.3}O_{2.50(2)}$ oxygen-deficient sample (Fig. 8). A magnetic frustration is apparently introduced for this sample resulting from the high concentration of disordered oxygen vacancies. A similar frustration in the magnetic superexchange interactions, resulting from the dilution of the magnetic matrix with diamagnetic ions, the formation of oxygen vacancies randomly distributed in the cubic structure, and mixed oxidation states of the magnetic ion was seen previously in $Sr_2FeTiO_{6-\delta}$ [27], A_2FeMO_6 (A = Ca, Sr, Ba; M = Nb, Ta, Sb) [28] and $Ba_2In_{2-x}Co_xO_5$ [29]. It is worth noting that the spin-glass behavior of the $SrMn_{0.7}Ga_{0.3}O_{2.50(2)}$ sample is further evidence for its oxygen-vacancy disordered structure found by neutron diffraction measurements. A vacancy ordered structure would most likely result in long-range magnetic ordering, such as the G-type magnetic structure observed for most of the vacancy-ordered brownmillerite compounds (cf. Ref. [25]).

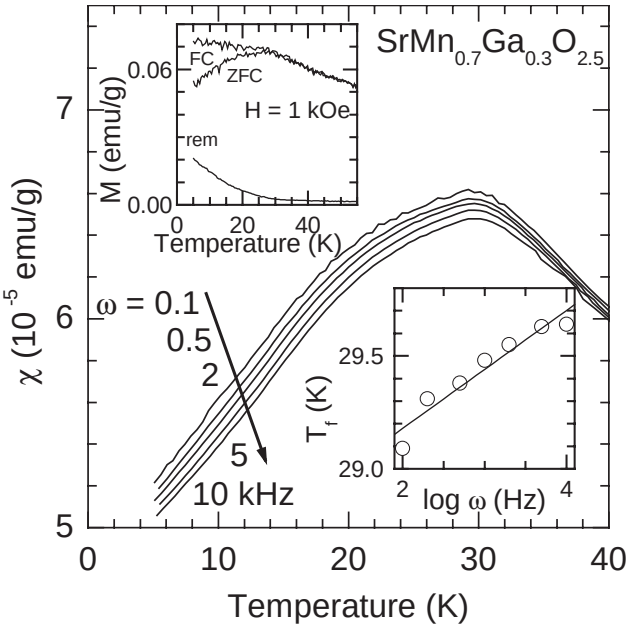

Fig. 8. Temperature dependences of the magnetic susceptibility of $SrMn_{0.7}Ga_{0.3}O_{2.5}$ measured for different frequencies in the AC magnetic field of 14 Oe. Lower inset is a log–log plot of the spin freezing temperature, T_f, as a function of frequency, ω. The straight line is a linear fit to the data. Upper inset shows the ZFC, FC, and remanent (rem) magnetizations.

3.3. The layer-ordered Sr_2MnGaO_5 and $Sr_2MnGaO_{5.5}$ compounds

Studies of the layer-ordered compound $Sr_2MnGaO_{5+\delta}$ have been reported by several authors in the last 2 years. These reports have focused on the reduced composition with $\delta \approx 0$ and the oxidized composition with $\delta \approx 0.5$—the same two compositions studied in the present work. Both the reduced and oxidized compositions were first studied by Abakumov et al. [16]. For a sample of composition $Sr_2MnGaO_{4.97}$, they reported a brownmillerite-type structure, orthorhombic space group *Ima*2, based on Rietveld refinement using X-ray powder diffraction data. For an oxidized composition of $Sr_2MnGaO_{5.47}$ they reported a tetragonal crystal structure, space group $P4/mmm$. Based on magnetic susceptibility measurements, they concluded that both compounds were canted antiferromagnets with ordering temperatures, T_N, of ~150 and 80 K, respectively. Wright et al. [19] studied the reduced compound by neutron powder diffraction and concluded that the crystal structure was better described by space group *Icmm*. The subtle difference in space group was explained to result from the ordering of oxygen vacancies in a different way than originally proposed. Their neutron powder diffraction data also confirmed the G-type antiferromagnetic ordering at low temperature. Most recently, Pomjakushin et al. [20] reported neutron powder diffraction results for both reduced and oxidized compositions, $Sr_2GaMnO_{5+\delta}$ ($\delta = 0.01$ and 0.52). For the reduced composition, $\delta = 0.01$, they found the same crystallographic space group as reported by Wright et al. [19] and G-type antiferromagnetic

ordering below a transition temperature of ~180 K. For the oxidized composition, $\delta = 0.52$, they reported a refinement of the crystal structure in tetragonal space group $P4/mmm$, but commented that they observed one small diffraction peak that should be extinct for this symmetry, suggesting the possibility of a lower-symmetry space group. Upon decreasing temperature, they observed diffuse scattering consistent with short-range (~40 Å coherence length) G-type antiferromagnetic ordering, beginning at ~180 K, followed by sharp magnetic peaks consistent with long-range C-type antiferromagnetic ordering beginning at ~100 K. In both magnetic structures, the Mn magnetic moments are coupled antifferomagnetically in the MnO_2 planes, but the mutual coupling of the MnO_2 planes is either antifferomagnetic (G-type), or ferromagnetic (C-type). Pomjakushin et al. [20] present a theoretical explanation for the local coexistence of C- and G-type related interactions in $Sr_2MnGaO_{5.5}$ involving the interplay of "diagonal" and "vertical" interlayer antifferomagnetic superexchange interactions between Mn^{4+} ions. The "vertical" (diagonal) interactions give rise to the G- (C-) type magnetic structures [20]. They conclude that local fluctuations in the intra-layer magnetic coupling lead to the short-range G-type correlations.

The present study of the reduced compound gives results for both the crystal and magnetic structures that agree with the work of Wright et al. [19] and Pomjakushin et al. [20]. The Rietveld refinement profile is shown in Fig. 9(a). Refined structural parameters are summarized in Table 3. Selected bond-length and angles are summarized in Table 4. ZFC and FC measurements of the DC molar susceptibility as a function of temperature (not shown) showed characteristics similar to those previously reported—a Curie–Weiss behavior above 200 K and a clear antiferromagnetic-like transition at 162(5) K. Additional reflections observed in the LT neutron diffraction data of $Sr_2MnGaO_{5.00(4)}$ index in the $Icm'm'$ magnetic space group [19,30] which corresponds to a G-type antiferromagnetic structure of the Mn sublattice, with moments aligned along the long-axis, b. The net Mn ordered magnetic moment determined from the Rietveld refinement of the model to the LT neutron diffraction data is 2.67(2) μ_B (Table 3).

Neutron powder diffraction data were collected at room temperature for two oxidized samples, called ox380 and ox800 (Table 1), which differed only in the final annealing temperature in oxygen before slowly cooling to room temperature. Initial Rietveld refinements were done with the previously reported tetragonal, $P4/mmm$ model. However, the data for the ox380 sample show selective peak broadening and the data for the ox800 sample showed peak splitting consistent with an orthorhombic cell (Fig. 10(a)–(d)). Since no ordering scheme of oxygen vacancies was found in our data, we

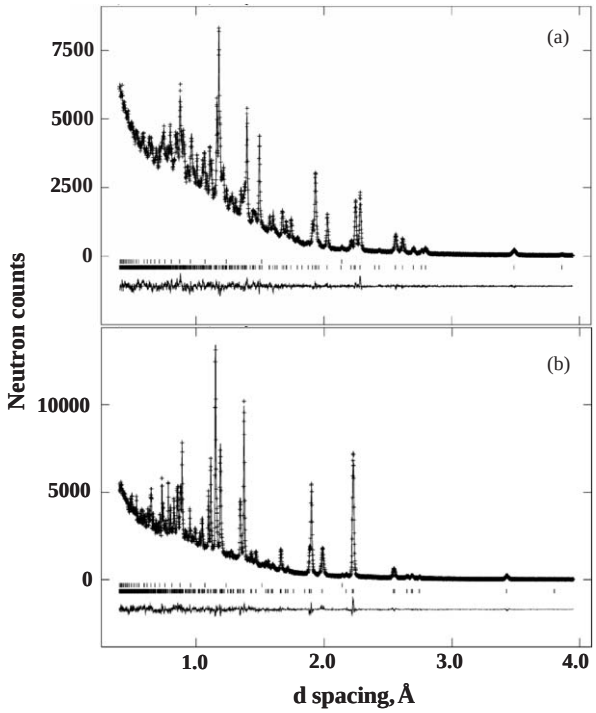

Fig. 9. Best-fit Rietveld refinement using TOF neutron powder diffraction data at RT for (a) Sr_2MnGaO_5 and (b) $Sr_2MnGaO_{5.5}$. Plus signs are observed data from Bank1 ($2\theta = 144.85°$), and continuous lines are calculated profile and difference. The upper series of tick marks correspond to Bragg peaks of the vanadium sample holder. For structural details see Table 3.

used the oxygen-vacancy disordered structure described by the orthorhombic $Cmmm$ space group to perform Rietveld refinements. Of the orthorhombic subgroups of $P4/mmm$ this space group describes the data best. Refined structural parameters for both samples are presented in Table 3. The improvement in goodness-of-fit parameters for the $Cmmm$ model was substantial: For $Cmmm$, $R_{wp} = 4.85\%$; $\chi^2 = 2.506$ (23 structural variables); while, for $P4/mmm$, $R_{wp} = 4.94\%$; $\chi^2 = 2.595$ (for 19 variables). The ability to see this orthorhombic distortion stems from the sharper diffraction peaks of the ox800 sample. As shown in Table 3, the refined orthorhombic distortion is actually the same for both samples. The higher oxygen annealing temperature for the ox800 sample may decrease strains, resulting in sharper diffraction peaks. Moreover, the time-of-flight diffraction method is well suited for detecting this small orthorhombic distortion because high resolution is obtained at large d spacing.

This structure consists of alternating layers of complete MnO_6 octahedra and oxygen-deficient $GaO_{5.5}$ "octahedra", where the oxygen vacancies are disordered in a $GaO_{1.5}$ plane (Fig. 11; Table 3). The process of filling the oxygen vacancies in the GaO_4 tetrahedral layer of the "parent" brownmillerite phase causes the lattice unit cell to shrink along the long axis in

Table 3
Structural and magnetic parameters of Sr_2MnGaO_5 and $Sr_2MnGaO_{5.5}$ at RT (~295 K) and LT (~12 K)

		Sr_2MnGaO_5		$Sr_2MnGaO_{5.5}$		
		RT	LT	"ox380"		"ox800"
				RT	LT	RT
a (Å)		5.5260(1)	5.5132(1)	5.3834(2)	5.3709(2)	5.3840(1)
b (Å)		16.1953(3)	16.1846(3)	5.3652(2)	5.3537(2)	5.3641(1)
c (Å)		5.3980(1)	5.3834(1)	7.9448(2)	7.9113(2)	7.9459(2)
V (Å^3)		483.09(1)	480.36(1)	229.468(4)	227.483(5)	229.477
Sr	x	0.5094(3)	0.5094(2)	—	—	—
	y	0.11134(7)	0.11110(6)	—	—	—
	z	—	—	0.2351(2)	0.2351(2)	0.2355(2)
	B (Å^2)	0.43(2)	0.11(2)	0.90(3)	0.60(3)	0.85(4)
Mn/Ga1	SOF	0.99(1)/0.01(1)	0.99/0.01	0.966(3)/0.034(3)	0.966/0.034	0.963(4)/0.037(4)
	B (Å)	1.17(9)	0.85(5)	0.52(6)	0.36(4)	0.48(8)
	Magnetic structure	—	G-type	—	20(3)% G-type 80(3)% C-type	—
	m_{Mn} (μ_B)	—	2.67(2)	—	1.48(3)	—
Ga/Mn2	SOF	0.467(2)/0.033(2)	0.467/0.033	0.479(2)/0.021(2)	0.479/0.021	0.480(2)/0.020(2)
	x	0.0648(4)	0.0652(3)	0.0434(7)	0.0422(7)	0.0442(9)
	z	−0.0316(8)	−0.0339(6)	—	—	—
	B (Å^2)	1.09(8)	0.64(5)	1.44(8)	1.22(6)	1.5(1)
O1	y	0.0053(1)	0.0050(1)	—	—	—
	U_{11} (Å^2)	1.20(8)	1.07(7)	0.34(8)	0.14(7)	0.4(1)
	U_{22} (Å^2)	0.95(8)	0.50(6)	0.78(9)	0.50(7)	0.7(1)
	U_{33} (Å^2)	0.63(6)	0.48(6)	1.04(7)	0.28(5)	1.04(9)
	U_{12} (Å^2)	—	—	−0.12(7)	−0.03(6)	−0.09(9)
	U_{13} (Å^2)	−0.66(6)	−0.56(5)	—	—	—
O2	SOF	0.5	0.5	—	—	—
	x	−0.0398(3)	−0.0394(3)	—	—	—
	y	0.1461(1)	0.14581(9)	—	—	—
	z	−0.0239(8)	−0.0203(8)	0.2464(2)	0.2471(2)	0.2468(2)
	U_{11} (Å^2)[a]	1.17(5)	0.84(4)	1.3(1)	1.1(1)	0.8(1)
	U_{22} (Å^2)	—	—	0.6(1)	−0.03(9)	1.2(2)
	U_{33} (Å^2)	—	—	2.0(1)	2.0(1)	2.5(2)
O3	SOF	0.5	0.5	0.372(2)	0.372	0.381(3)
	x	0.3732(6)	0.3741(5)	0.205(1)	0.206(1)	0.204(1)
	y	—	—	0.296(1)	0.297(1)	0.295(1)
	z	0.8724(6)	0.8753(6)	—	—	—
	B (Å)	1.80(9)	1.27(7)	1.60(9)	1.39(6)	1.9(1)
R_{wp} (%)		3.96	4.04	4.85	4.58	4.42
R_{exp} (%)		2.82	2.69	3.06	3.10	3.40

Rietveld analyses with neutron powder diffraction data were done using: (1) For Sr_2MnGaO_5 the orthorhombic space group *Icmm*, with the following atom positions: Sr at $8h(x,y,0)$, Mn/Ga at $4a(0,0,0)$, Ga/Mn and O3 at $8i(x,1/4,z)$, O1 at $8g(1/4,y,1/4)$, and O2 at $16j(x,y,z)$. The magnetic structure was modeled using the magnetic space group $Icm'm'$; (2) For $Sr_2MnGaO_{5.5}$ the orthorhombic space group *Cmmm*, with the following atom positions: Sr at $4l(1/2,0,z)$, Mn/Ga1 at $2a(0,0,0)$, Ga/Mn2 at $4h(x,0,1/2)$, O1 at $4e(1/4,1/4,0)$, O2 at $4k(0,0,z)$ and O3 at $8q(x,y,1/2)$. The magnetic structures were modeled using the magnetic space groups $C_Pm'm'm$ (C-type) and $C_Pm'm'm$ (G-type); m_{Mn} is the Mn ordered magnetic moment. For $Sr_2MnGaO_{5.5}$ m_{Mn} of C- and G-type AF structures were constrained to the same value. O3 SOF of $Sr_2MnGaO_{5.5}$ at LT was fixed to the values obtained from the RT refinement. RT Mn/Ga1 and Ga/Mn2 SOF values were obtained by constraining the total site occupancy to one. LT SOF values were fixed to the corresponding RT ones. See caption of Table 1 for more information.

[a] For O2 in Sr_2MnGaO_5, B (Å^2) values are given.

$Sr_2MnGaO_{5.5}$. The refined site occupation values for the oxygen sites in the Ga plane (O3, Table 3), are 0.372(2) and 0.381(3) which correspond to the compositions $Sr_2MnGaO_{5.49(1)}$ and $Sr_2MnGaO_{5.52(1)}$ for the "ox380" and "ox800" samples, respectively. This is in excellent agreement with the oxygen-content values obtained by

Table 4
Selected bond lengths (Å) and bond angles (deg) for Sr_2MnGaO_5, and $Sr_2MnGaO_{5.5}$ at RT (~295 K)

	Sr_2MnGaO_5	$Sr_2MnGaO_{5.5}$ "ox380"	$Sr_2MnGaO_{5.5}$ "ox800"
Sr–O1	2.613(2)[×2] 2.675(2)[×2]	2.6643(9)[×4]	2.667(1)[×4]
Sr–O2	2.557(2)[×2] 2.636(4)[×2] 2.888(4)[×2]	2.6841(1)[×2] 2.6932(1)[×2]	2.6836(1)[×2] 2.6935(1)[×2]
Sr–O3	2.467(2)[×2]	2.615(2)[×4] 3.079(2)[×4]	2.614(2)[×4] 3.077(3)[×4]
Mn/Ga1–O1	1.93311(9)[×4]	1.90010(4)[×4]	1.90001(3)[×4]
Mn/Ga1–O2	2.380(2)[×2]	1.958(1)[×2]	1.961(2)[×2]
Ga/Mn2–O2	1.780(2)[×2]	2.028(1)[×2]	2.026(2)[×2]
Ga/Mn2–O3 (CN4)	1.872(5), 1.908(4)	1.741(8), 1.812(8)	1.745(9), 1.802(9)
Ga/Mn2–O3 (CN6)		1.741(8), 1.812(8) 2.077(8), 2.125(8)	1.745(9), 1.802(9) 2.072(9), 2.136(9)
Mn/Ga1–O1–Mn/Ga1	175.0(1)	180.0	180.0
Mn/Ga1–O2–Ga/Mn2	152.69(9), 155.67(9)	173.4(1)	173.3(1)
Ga/Mn2–O3–Ga/Mn2	118.8(2), 117.5(2) 125.7(2), 127.3(2)	149.6(3), 157.6(2) 161.0(1), 169.0(2)	149.5(3), 157.5(2) 161.1(2), 169.2(3)

For the Ga/Mn2–O3 distances, CN4 and CN6 are the equatorial bond lengths for the tetrahedral and octahedral coordinations, respectively.

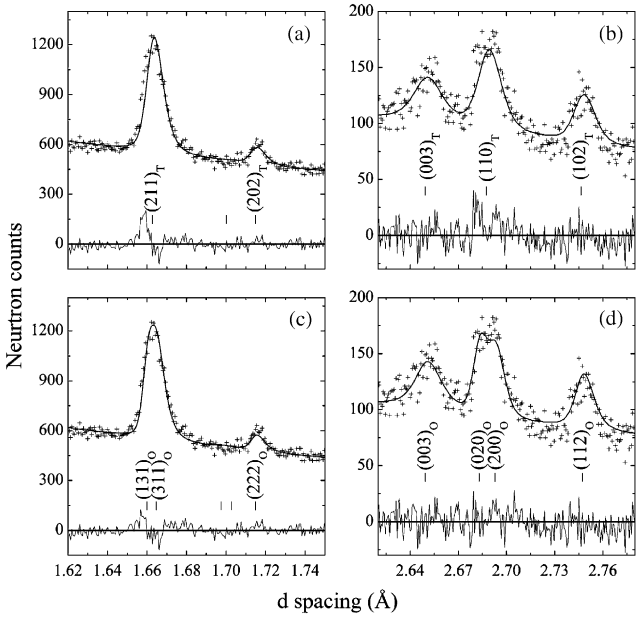

Fig. 10. Selected best-fit Rietveld refinement using TOF neutron powder diffraction data at RT for the $Sr_2MnGaO_{5.5}$ "ox800" sample. (a,b) show the refinement of the tetragonal *P4/mmm* model, and (c,d) show the refinement of the orthorhombic *Cmmm* model. Plus signs are observed data, and continuous lines are calculated profile and difference.

TGA measurements for these samples. Selected bond-lengths and angles are summarized in Table 4. All interatomic distances are well within the range for Ga^{3+}–O, Mn^{4+}–O, and Sr^{2+}–O distances in inorganic compounds tabulated in the Inorganic Crystal Structure Database [31].

The use of the *Cmmm* space group to describe the structure of the $Sr_2MnGaO_{5.5}$ compounds may be considered only as the first step towards the solution of the actual structure. Our data show unequivocally the occurrence of an orthorhombic distortion in these samples, ruling out the *P4/mmm* structure. However, the *Cmmm* model does not reveal a physical reason for this distortion to exist. An oxygen-vacancy ordered structure may be present here; yet, with such a small orthorhombic distortion, and with the data presented here it was impossible to find this ordering scheme. A recent paper on the oxygen-vacancy ordered structures in $SrFeO_{3-\delta}$ [25] illustrates how difficult it can be to determine the correct space groups for such compounds. In those compounds, complex patterns of oxygen-vacancy ordering result from the occurrence of Fe in either octahedral or pyramidal coordination. The formation of the same ordering configurations in the case of oxidized $Sr_2MnGaO_{5.5}$ is unlikely because pyramidal coordination is not characteristic of Ga^{3+}. The only example of an inorganic structure with five-coordinated Ga^{+3} is reported in Ref. [32] where, from X-ray powder diffraction data, it is concluded that "this is the first example of Ga with this coordination configuration in an extended structure". Moreover, the high stability of oxygen coordination of Ga^{+3} with spherical symmetry is supported by the reports of high-pressure phase transitions in gallates with an increase of Ga^{+3} coordination number which are related to switching from tetrahedral coordination directly to octahedral coordination [33–35].

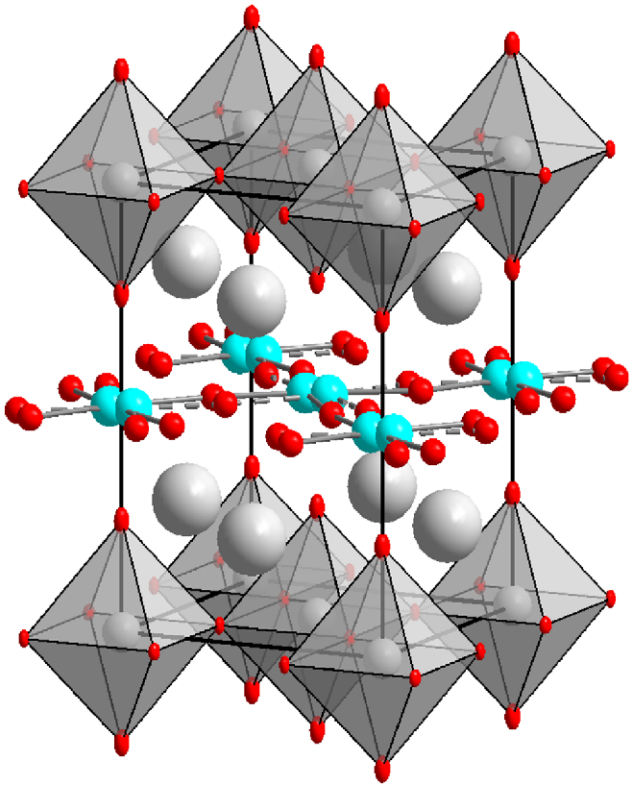

Fig. 11. Unit cell of $Sr_2MnGaO_{5.5}$ (space group *Cmmm*). Large spheres represent Sr; spheres inside octahedra represent Mn; light spheres between octahedra layers represent Ga. Oxygen atoms are represented by the remaining spheres.

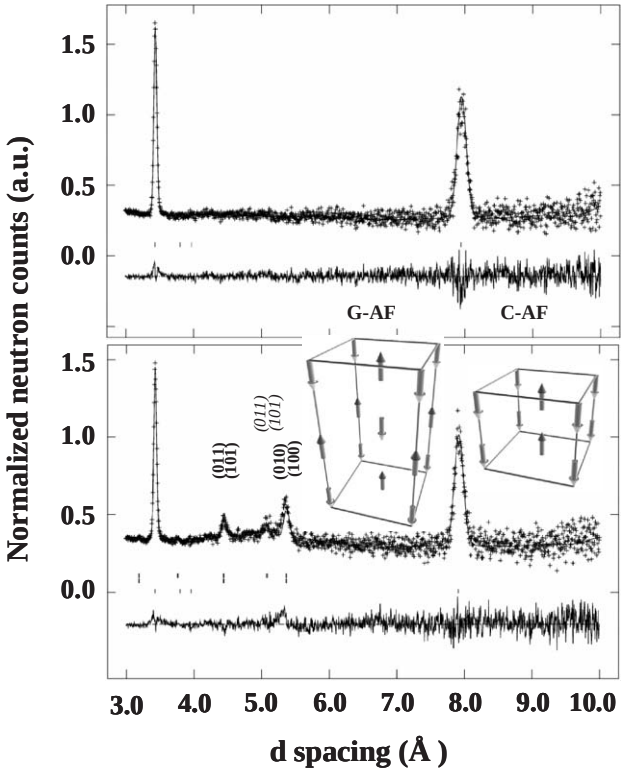

Fig. 12. Best-fit Rietveld refinement using TOF neutron powder diffraction data at RT (upper panel) LT (lower panel) for the $Sr_2MnGaO_{5.5}$ "ox380" sample. Plus signs are observed data from Bank3 ($2\theta = 44°$), and continuous lines are calculated profile and difference. Observed data is normalized to the incident beam. The upper, middle and lower series of tick marks correspond to magnetic G- type, C-type, and crystallographic Bragg positions, respectively. **Bold**, and *Italic* indices correspond to C- and G-type magnetic reflections with finite intensity, respectively (see text). The C- and G-type antiferromagnetic structures are also shown. For structural and magnetic details see Table 3.

Another, hypothetical ordered model consisting of the layer sequence –OOOT– (–MnO_2–GaO_2–MnO_2–GaO–) has been proposed previously for the layer-ordered $A_2MnGaO_{5.5}$ compounds [16,36] but has never been observed experimentally by diffraction methods. This model is inconsistent with the present neutron diffraction data, generating additional reflections with significant calculated intensity not observed in the diffraction pattern. The present diffraction data show no superlattice peaks which would give evidence for these, or other, vacancy ordered structures. Hence, the structure is reported in orthorhombic space group *Cmmm* with disordered oxygen vacancies.

The AC susceptibility, χ, vs. temperature for $Sr_2MnGaO_{5.49(1)}$ is shown in Fig. 6(a). As reported by Pomjakushin et al. [20], the magnetic properties of this sample are complicated by the presence of two antiferromagnetic phases with highly anisotropic interactions within the Mn–O planes and perpendicular to the planes.

Our LT neutron diffraction data for the $Sr_2MnGaO_{5.49(1)}$ ox380 sample show additional reflections not observed at RT (cf. Fig. 12). These reflections were assumed to be of magnetic origin. Attempts to describe their relative intensities using a single magnetic unit cell were not successful, even when using unusually high axis multiplications of the crystallographic cell. In agreement with the work of Pomjakushin et al. [20], the extra reflections can be indexed as two orthogonal sets of magnetic origin. One set is described using the $C_Im'm'm$ magnetic space group [30], and corresponds to the G-type antiferromagnetic structure of the Mn sublattice (Fig. 12), and the other set is described using the $C_Pm'm'm$ magnetic space group [30], corresponding to the C-type antifferomagnetic structure of the Mn sublattice (Fig. 12). It should be noted that both magnetic structures are consistent with the *Cmmm* crystal structure reported here. The Mn moments are directed parallel to the *c*-axis. A two-phase Rietveld refinement of the C- and G-type phase fractions and ordered moment for each phase is not possible because the problem is underdetermined; hence a constraint is required. Since the in-plane magnetic interactions are identical in both structures, and only the sign between the layers is different, it is assumed that both structures have the same ordered magnetic moments. This same assumption was made in the analogous case of the

coexisting C and C* magnetic structures in $La_{2-2x}Sr_{1+2x}Mn_2O_7$ ($0.74<x<0.92$) [37]. With this constraint, the magnitude of the Mn^{4+} magnetic moment in $Sr_2MnGaO_{5.49(1)}$ was refined to $1.48(3)\,\mu_B$ (Table 3). In addition, relative abundances of 20(3)% and 80(3)% were obtained for G- and C-type structures, respectively (Table 3). A broad diffuse scattering peak is also observed, approximately centered at the same position of the most intense G-type reflections ({101} and {011}, Fig. 12(b)). This diffuse scattering peak is absent in the RT data (Fig. 12(a)) and can be attributed to a short-range magnetic ordering of mainly the G-type phase. The reduced ordered magnetic moment found for the Mn^{4+} ions in $Sr_2MnGaO_{5.5}$ (compared to the expected spin-only value of $3\,\mu_B$ for Mn^{4+}) is in agreement with the existence of short-range ordered magnetic structure. The significant difference between our results (Fig. 12), and those reported by Pomjakushin et al. [20], is the clear existence of a long-range G-type ordering in our data, and its absence in their data.

4. Conclusions

The initial goal of this work was to explore the ability to stabilize $SrMnO_{3-\delta}$ in the perovskite phase by substituting Ga for Mn and to determine the properties of these new solid solution compounds. It was found that $SrMn_{1-x}Ga_xO_{3-\delta}$ can be made in the perovskite phase for $0\leqslant x\leqslant 0.33$ if a two-step synthesis procedure is used. Initial synthesis is done at 1300–1335°C in reducing atmosphere. When these samples are cooled without allowing oxygen uptake, they remain in the perovskite phase, with the oxygen-vacancy content being at or near the limit defined by the +3 valence state for Mn; i.e., $\delta\approx 0.5$. These oxygen-deficient samples can then be oxygenated by heating in oxygen or air at 450°C and slowly cooling. At this low annealing temperature, cation diffusion is not thermally enabled. Thus, the samples do not decompose even though the tolerance factor departs from the conditions required for the perovskite structure as oxygen is added and the Mn valence (and its ionic size) changes. The maximum oxygen contents are defined by the +4 valence state for the Mn; thus, $\delta\approx x/2$ for the maximally oxygenated samples.

For the maximally oxygenated compositions of the perovskite phase solid solution, $SrMn_{1-x}Ga_xO_{3-\delta}$ ($0\leqslant x\leqslant 0.33$, $\delta\approx x/2$), transformation to a G-type antiferromagnetic ordering of the Mn spins occurs at low temperature, with the transition temperature decreasing linearly from 233(2) K at $x=0$ to 105(2) K at $x=0.3$. For the reduced samples, and Ga concentrations near the solubility limit, the magnetic ordering is destroyed, leading to a spin-glass state at low temperature. This is thought to result because both Ga and the oxygen vacancies are disordered. The failure for oxygen vacancies to order when sufficient Ga is substituted on the Mn site is thought to be a manifestation of the inability of Ga^{3+} to adopt a five coordinated pyramidal configuration that occurs in many other vacancy ordering schemes in systems such as $SrFeO_{3-\delta}$, and $SrMnO_{3-\delta}$ [10,25]. Introducing an increasing amount of Ga^{3+} into the oxygen-deficient $SrMnO_{2.5}$ compound, which has all Mn^{3+} in five coordinated square pyramid configuration [10], interferes with this particular ordering scheme of the oxygen vacancies since a pyramidal five coordinated site is not available for Ga^{3+}. Thus, if the initial synthesis at high temperature results in a random distribution of Ga on the Mn site, and Ga is not able to diffuse at lower temperatures (e.g., the oxygen annealing temperatures), the oxygen vacancies cannot order.

For Ga contents beyond $x\approx 0.33$, mixed-phase samples are formed until the previously known [16,19,20] layer-ordered phase $Sr_2MnGaO_{6-\delta}$ ($0.5\leqslant\delta\leqslant 1.0$) is formed at $x=0.5$. In this phase, the Ga ions and Mn ions order into layers. These compounds have been studied previously. However, our work gives slightly different results. We find that the maximally oxygenated layer-ordered phase, $Sr_2MnGaO_{5.5}$, displays a small orthorhombic distortion, rather than tetragonal symmetry (space group $P4/mmm$) as previously reported [20]. The ability to observe this small orthorhombic distortion perhaps results from achieving sharper diffraction peaks by optimizing the oxygen annealing procedure. The orthorhombic structure is refined in the *Cmmm* space group, which gives the best fit among the subgroups of $P4/mmm$. There is no obvious explanation for why the orthorhombic distortion occurs. Given that the orthorhombic distortion is so small, it is possible that a different space group, perhaps with oxygen-vacancy ordering, would be a more correct model, but the present data do not allow this to be investigated in an exhaustive way. Some previously proposed ordered models [25,36] were tested and failed. It is, of course, possible that oxygen-vacancy ordering is absent in the layer-ordered compound for the same reason it is absent in the perovskite solid solutions; i.e., the inability of Ga^{3+} to adopt a five coordinated site. The comparison of $Sr_2MnGaO_{5.5}$ with $Sr_2Fe_2O_{5.5}$ supports this possibility, where the latter ordering scheme involves five coordinated Fe^{3+} ions [25]. If no vacancy ordering is present in the Ga-substituted compound, the *Cmmm* space group is likely to be correct.

The present samples of the maximally oxygenated layer-ordered compounds also display slightly different magnetic ordering than previously reported. In previous work, a coexistence of long-range C-type magnetic ordering and short-range (~40 Å) G-type magnetic ordering was reported. The competition of these

magnetic ordering schemes was explained in terms of interplay of "diagonal" and "vertical" interlayer antiferromagnetic superexchange interactions between Mn^{4+} ions. In the present work, the same coexistence of two magnetic ordering schemes is observed, but both show long-range coherence. We do not have an explanation for this difference, but suspect it may result from the different oxygen annealing procedures used in the present study. If this is the case, the present result illustrates the delicate nature of the competition between these two magnetic ordering patterns.

Acknowledgments

Work at NIU was supported by the NSF-DMR-0302617 and by the State of Illinois under HECA. At ANL, work was supported by the US Department of Energy, Division of Basic Energy Science—Materials Sciences, under contract No. W-31-109-ENG-38.

References

[1] Y. Tokura, N. Nagaosa, Science 288 (5465) (2000) 462–468.
[2] A. Urushibara, Y. Moritomo, T. Arima, A. Asamitsu, G. Kido, Y. Tokura, Phys. Rev. B 51 (1995) 14103.
[3] P. Schiffer, A.P. Ramirez, W. Bao, S.-W. Cheong, Phys. Rev. Lett. 75 (1995) 3336.
[4] H.Y. Hwang, S-W. Cheong, P.G. Radaelli, M. Marezio, B. Batlogg, Phys. Rev. Lett. 75 (1995) 914–917.
[5] F. Millange, V. Caignaert, B. Domenges, B. Raveau, E. Suard, Chem. Mater. 10 (1998) 1974.
[6] O. Chmaissem, B. Dabrowski, S. Kolesnik, M. Mais, D.E. Brown, J.D. Jorgensen, S. Short, Phys. Rev. B 67 (2003) 094431.
[7] B. Dabrowski, O. Chmaissem, J. Mais, S. Kolesnik, J.D. Jorgensen, S. Short, Mater. Res. Soc. Symp. Proc. 718 (2002) 169.
[8] T. Negas, R.S. Roth, J. Solid State Chem. 1 (1970) 409.
[9] R.D. Shannon, Acta Crystallogr. A 32 (1976) 751.
[10] V. Caignaert, J. Magn. Magn. Mater. 166 (1997) 117.
[11] K.R. Poeppelmeier, M.E. Loenowicz, J.C. Scanion, J.M. Longo, W.B. Yelon, J. Solid State Chem. 45 (1982) 71.
[12] B. Dabrowski, O. Chmaissem, J. Mais, S. Kolesnik, J.D. Jorgensen, S. Short, J. Solid State Chem. 170 (2003) 154.
[13] J. Mais, B. Dabrowski, S. Kolesnik, O. Chmaissem, Unpublished.
[14] M. Patrakeev, et al., Private communication.
[15] V.V. Kharton, A.L. Shaulo, A.P. Viskup, M. Avdeev, A.A. Yaremchenko, M.V. Patrakeev, A.I. Kurbakov, E.N. Naumovich, F.M.B. Marques, Solid State Ionics 150 (2002) 229.
[16] A.M. Abakumov, M.G. Rozova, B.Ph. Pavylyuk, M.V. Lobanov, E.V. Antipov, O.I. Lebedev, G. Van Tendeloo, D.V. Sheptyakov, A.M. Balagurov, F. Bourée, J. Solid State Chem. 158 (2001) 100.
[17] A.M. Abakumov, M.G. Rozova, B.Ph. Pavlyuk, M.V. Lobanov, E.V. Antipov, O.I. Lebedev, G. Van Tendeloo, O.L. Ignatchik, E.A. Ovtchenkov, Yu.A. Koksharov, A.N. Vasil'ev, J. Solid State Chem. 160 (2001) 353.
[18] A.J. Wright, H.M. Palmer, P.A. Anderson, C. Greaves, J. Mater. Chem. 11 (2001) 1324.
[19] A.J. Wright, H.M. Palmer, P.A. Anderson, C. Greaves, J. Mater. Chem. 12 (2002) 978.
[20] V.Yu. Pomjakushin, A.M. Balagurov, T.V. Elzhov, D.V. Sheptyakov, P. Fischer, D.I. Khomskii, V.Yu. Yushankhai, A.M. Abakumov, M.G. Rozova, E.V. Antipov, M.V. Lobanov, S. Billinge, Phys. Rev. B 66 (2002) 184412.
[21] P.D. Battle, A.M.T. Bell, S.J. Blundell, A.I. Coldea, D.J. Gallon, F.L. Pratt, M.J. Rosseinsky, C.A. Steer, J. Solid State Chem. 167 (2002) 188.
[22] J.D. Jorgensen, J. Faber Jr., J.M. Carpenter, R.K. Crawford, J.R. Haumann, R.L. Hitterman, R. Kleb, G.E. Ostrowsky, F.J. Rotella, T.G. Worlton, J. Appl. Crystallogr. 22 (1989) 321.
[23] A.C. Larson, R.B. Von Dreele, Los Alamos National Laboratory, LAUR 86-748, 1994.
[24] B.H. Toby, J. Appl. Crystallogr. 34 (2001) 210.
[25] J.P. Hodges, S. Short, J.D. Jorgensen, X. Xiong, B. Dabrowski, S.M. Mini, C.W. Kimball, J. Solid State Chem. 151 (2000) 190.
[26] J.A. Mydosh, Spin Glasses: An Experiment Introduction, Taylor & Francis, London, 1993.
[27] T.C. Gibb, P.D. Battle, S.K. Bollen, R.J. Whitehead, J. Mater. Chem. 2 (1992) 111.
[28] P.D. Battle, T.C. Gibb, A.J. Herod, S.H. Kim, P.H. Munns, J. Mater. Chem. 5 (1995) 865.
[29] A.D. Lozano Gorrín, P. Núñez, M.A. López de la Torre, J. Romero de Paz, R. Sáez Puche, J. Solid State Chem. 165 (2002) 254.
[30] W. Opechowski, R. Guccione, in: G.T. Rado, H. Suhl (Eds.), Magnetism, Vol. IIA, Academic Press, New York, 1965, pp. 105–165.
[31] G. Bergerhoff, R. Hundt, R. Sievers, I.D. Brown, J. Chem. Inf. Comput. Sci. 23 (1983) 66.
[32] W.J. Zhu, P.H. Hor, Inorg. Chem. 36 (1997) 3576.
[33] Y.P. Zhou, X.F. Ma, X.W. Yan, S.L. Wen, J. Mater. Synth. Proc. 5 (1997) 4391997.
[34] J.L. Robeson, R.R. Winters, W.S. Hammack, Phys. Rev. Lett. 73 (1994) 1664.
[35] J. Badro, P. Gillet, P.F. McMillan, A. Polian, J.P. Itie, Europhys. Lett. 40 (1997) 533.
[36] J.-C. Grenier, F. Menil, M. Pouchard, P. Hagenmuller, Mater. Res. Bull. 13 (1978) 329.
[37] C.D. Ling, J.E. Millburn, J.F. Mitchell, D.N. Argyriou, J. Linton, H.N. Bordallo, Phys. Rev. B 62 (2000) 15096.